Journal of Crystal Growth 378 (2013) 454–458

Contents lists available at SciVerse ScienceDirect

Journal of Crystal Growth

journal homepage: www.elsevier.com/locate/jcrysgro

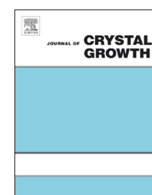

RF-MBE growth of cubic InN nano-scale dots on cubic GaN

Junichiro Suzuki*, Misao Orihara, Shuhei Yagi, Yasuto Hijikata, Hiroyuki Yaguchi

Graduate School of Science and Engineering, Saitama University, 255 Shimo-Ohkubo, Sakura-ku, Saitama 338–8570, Japan

ARTICLE INFO

Available online 31 December 2012

Keywords:
A1. Nanostructures
A3. Molecular beam epitaxy
B1. Nitrides
B2. Semiconducting indium compounds

ABSTRACT

This paper reports the first successful growth and structural control of cubic InN (c-InN) nano-scale dots. The samples were grown on MgO (0 0 1) substrates by RF-N_2 plasma molecular beam epitaxy (RF-MBE). Cubic GaN (c-GaN) underlayers with a thickness of 500 nm were grown on the substrates followed by the growth of a few nm-thick InN under various conditions. The formation of InN dots aligned along the ⟨1 1 0⟩ directions were confirmed by atomic force microscopy (AFM). X-ray diffraction (XRD) measurements suggested the cubic zincblende lattice structure of the obtained InN dots. The area density and size of c-InN dots were well controlled by adjusting the growth conditions such as the substrate temperature and the In flux, and a very high dot density of 2.2×10^{11} cm^{-2} was successfully obtained at a growth temperature of 470 °C and an In flux of 7.0×10^{-5} Pa.

© 2013 Elsevier B.V. All rights reserved.

1. Introduction

Heterostructures based on InN are expected for the use in optical devices such as high efficiency light emitting devices targeted for infrared region and multijunction solar cells covering the full range of the solar spectrum. From the view point of optical device application, semiconductor nanostructures such as quantum dots are very important. Strain-induced self-organized growth of nano-scale dots is one of the convenient methods to fabricate dots with high area density. There have been several reports on the self-organized growth of h-InN dots on h-GaN underlayers [1–3]. However, the growth of c-InN dots has not been reported to date. Although the most stable phase of InN is the hexagonal wurtzite structure (h-InN), InN is able to have the cubic zincblende structure (c-InN) as a metastable phase. Nitrides with the cubic crystalline structure have several advantages compared to those with the hexagonal structure in practical view. Different from hexagonal nitrides, their higher crystalline symmetry of the cubic nitrides results in isotropic properties and no spontaneous polarization induced-electric fields in the direction parallel to the *c*-axis. In addition, it is expected that cubic nitrides have superior electronic properties such as higher carrier mobilities, higher drift velocities and better doping efficiencies [4]. Furthermore, because the band gap energy of c-InN is 0.2 eV smaller than that of h-InN [5], c-InN extends the feasibility of band gap engineering based on nitride semiconductors. In this study, we have tried to grow c-InN dots on c-GaN and this paper reports on the first successful growth and structural control of self-organized c-InN dots.

2. Experimental details

Fig. 1 shows a schematic structure and the growth procedure of the samples fabricated in this study. The samples were grown on MgO (0 0 1) substrates by RF-N_2 plasma molecular beam

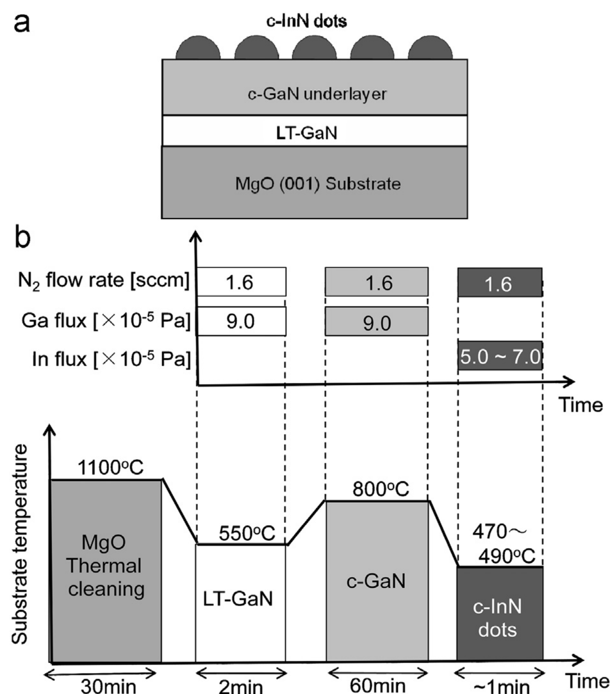

Fig. 1. (a) Sample structure and (b) growth procedure of c-InN dots.

* Corresponding author.
E-mail address: suzujun@opt.ees.saitama-u.ac.jp (J. Suzuki).

0022-0248/$ - see front matter © 2013 Elsevier B.V. All rights reserved.
http://dx.doi.org/10.1016/j.jcrysgro.2012.12.050

epitaxy (RF-MBE). First, the surface of MgO substrates was thermally cleaned for 30 min at 1100 °C. Then 15 nm-thick low temperature (LT)-GaN buffer layers were grown on the substrates at 550 °C followed by the growth of cubic GaN (c-GaN) underlayers with a thickness of 500 nm at 800 °C. For the GaN growth, Ga flux was fixed at 9.0×10^{-5} Pa. After that, InN was deposited to form dots under various growth conditions of substrate temperature (470–490 °C), In flux (5.0×10^{-5} Pa $-$ 7.0×10^{-5} Pa) and InN deposition amount (1.4–30 nm). During the growth, the plasma power and the N_2 flow rate were fixed at 350 W and 1.6 sccm, respectively.

Reflection high energy electron diffraction (RHEED) was used to evaluate *in-situ* growing surface conditions. The structural properties of fabricated InN dots were investigated by atomic force microscopy (AFM) and X-ray diffraction (XRD). The hexagonal phase content in the c-GaN underlayers was estimated from the relative XRD intensities of the cubic (0 0 2) and hexagonal (10–11) planes measured by ω-scan [6,7] and the value was less than 1% for all the samples.

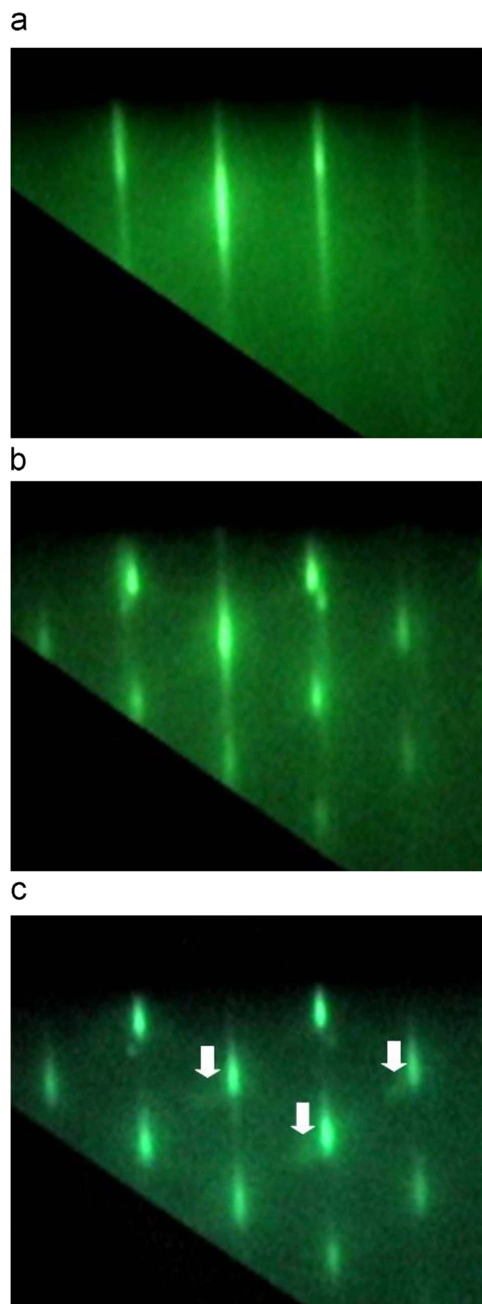

Fig. 2. *In-situ* RHEED images taken (a) before InN deposition (c-GaN surface) and (b), (c) after InN deposition with the thickness of 1.4 nm and 2.1 nm, respectively. The arrows in (c) indicates spots due to hexagonal phase inclusion or stacking faults along the (1 1 1) planes. The incident azimuth of the RHEED beam was ⟨1 1 0⟩ direction.

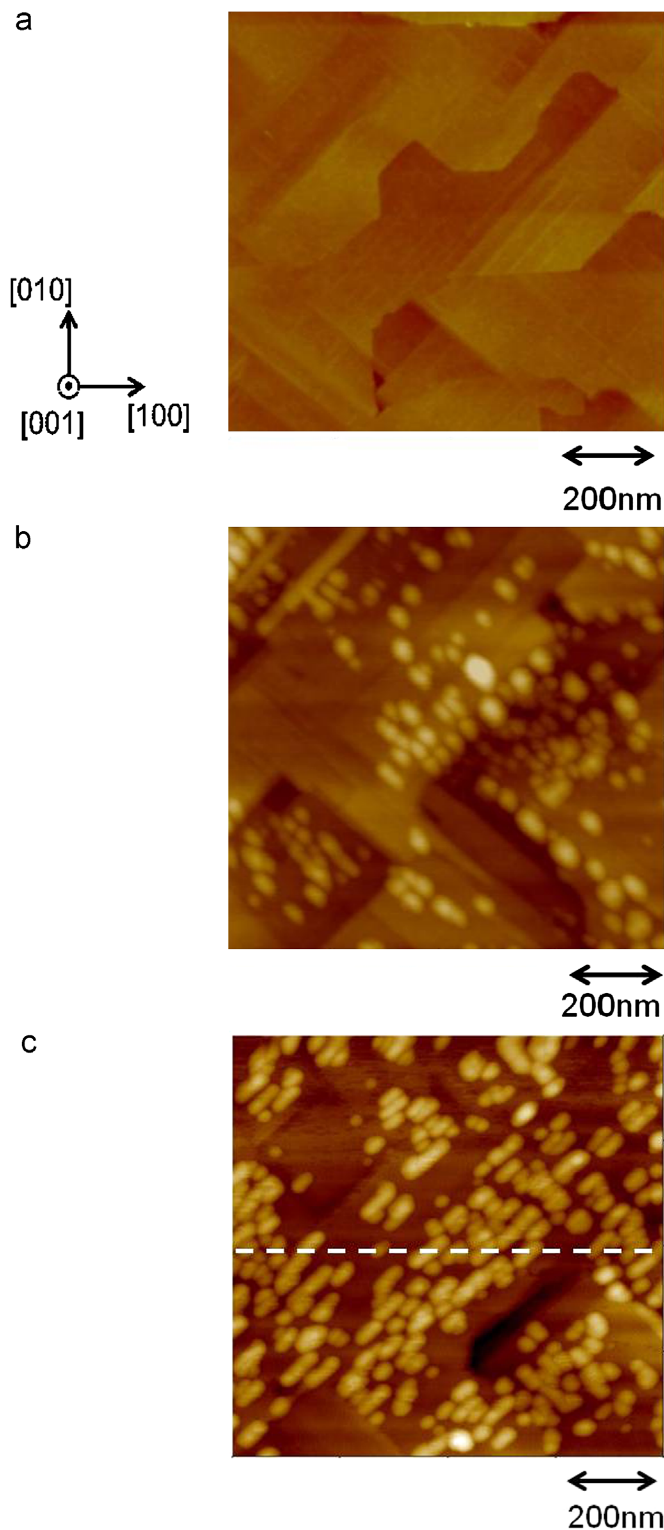

Fig. 3. AFM images of (a) before InN deposition (c-GaN surface) and (b), (c) after InN deposition with the thickness of 1.4 nm and 2.1 nm, respectively.

3. Results and discussion

3.1. Formation and structural evaluation of cubic InN dots

Fig. 2(a) shows a RHEED pattern taken just after the c-GaN deposition. Fig. 2(b) and (c) show those taken after the InN growth with the equivalent InN deposition thickness of 1.4 nm and 2.1 nm, respectively. The incident azimuth of the RHEED beam was ⟨1 1 0⟩ direction. The substrate temperature and the In flux during the InN growth were 490 °C and 5.0×10^{-5} Pa, respectively. Fig. 3(a)–(c) show AFM images (1 μm × 1 μm) of the sample surfaces which correspond to the RHEED patterns in Fig. 2(a)–(c), respectively.

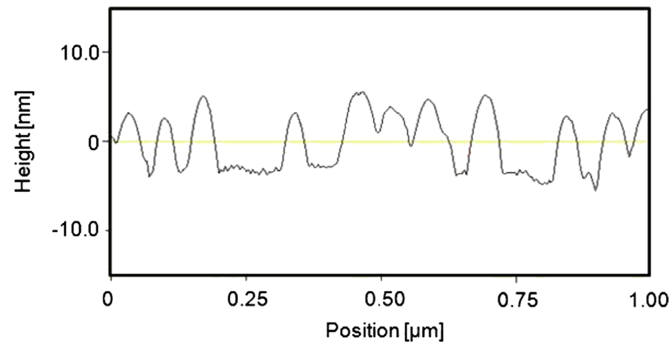

Fig. 4. AFM images of a cross section of c-InN dots.

The streak RHEED pattern in Fig. 2(a) and the AFM image in Fig. 3(a) in which clear step edges along the ⟨1 1 0⟩ directions are found with a small root mean square (RMS) roughness of 0.41 nm indicate that an atomically smooth surface of the c-GaN underlayer is obtained. The RHEED pattern gradually changed from streaks to a spot pattern with increasing InN deposition amount as shown in Fig. 2(b) and (c). The RHEED spots appeared a little inside the streak lines originate from the c-GaN surface as can be seen in Fig. 2(b). This indicates that the three-dimensional growth of strain released InN took place. The spot pattern represents the structural features of zincblende lattice [8,9]. After the InN deposition with the thickness of 2.1 nm, relatively weak diffraction spots implying the hexagonal phase inclusion or stacking faults along the (1 1 1) planes [8,10] were also observed in the RHEED pattern at the positions indicated by arrows in Fig. 2(c). However, XRD measurements suggested that the cubic phase is dominant in the deposited InN as indicated later in this

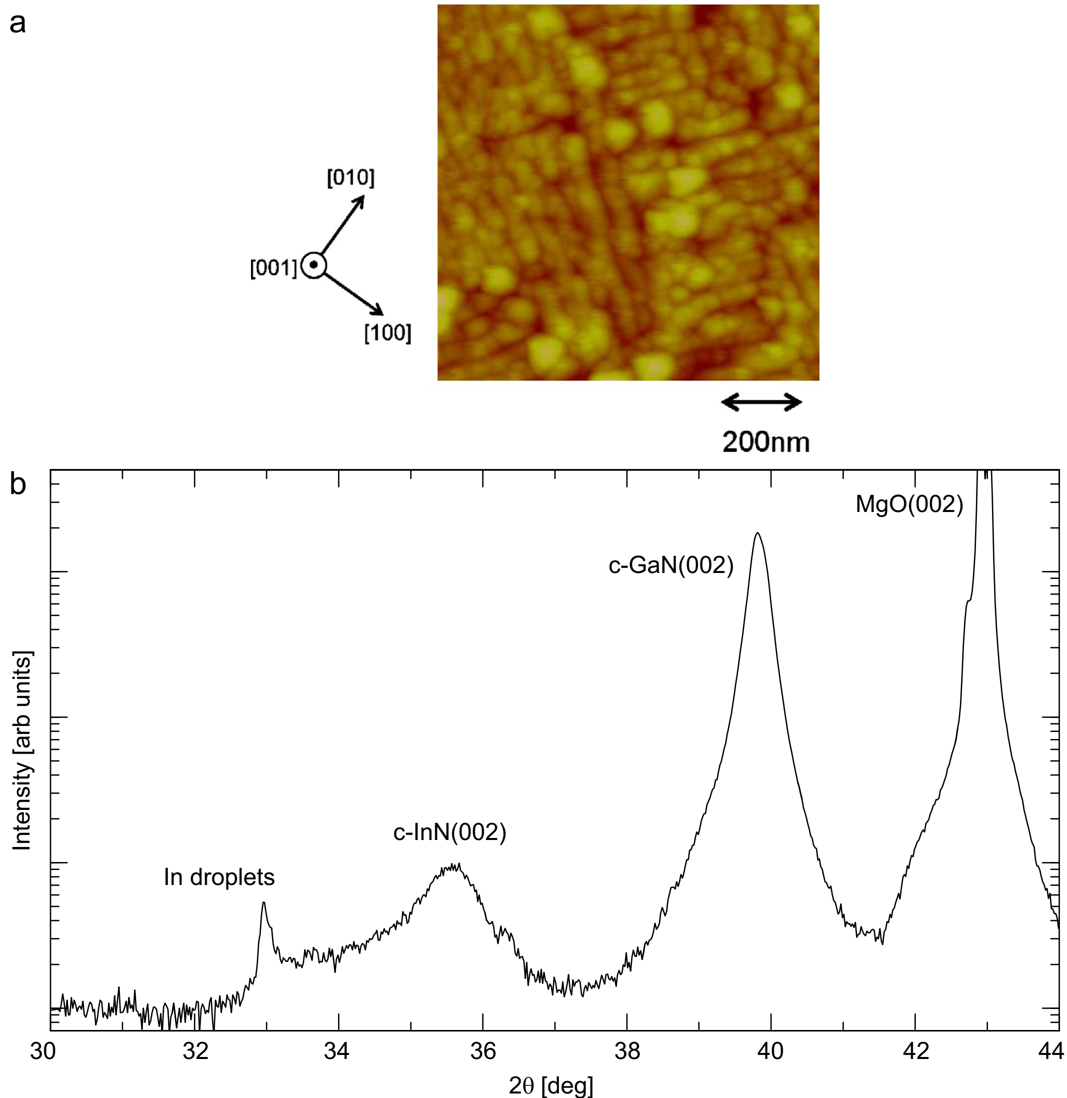

Fig. 5. (a) AFM image and (b) θ–2θ XRD pattern of InN dots grown with the InN deposition amount of 30 nm.

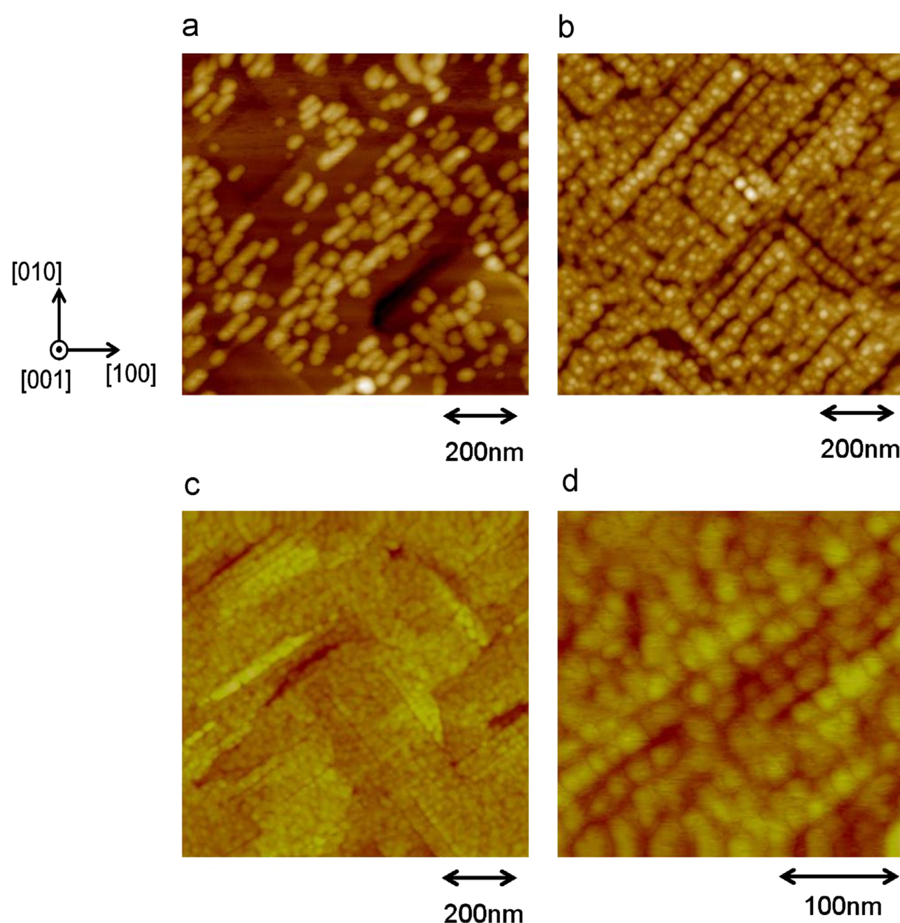

Fig. 6. AFM images of c-InN dots grown under various conditions. (d) is a magnified image of (c). The growth conditions of these dots are summarized in Table 1.

Table 1
The growth conditions of c-InN dots in Fig. 6(a)–(d).

Growth conditions	Growth temperature [°C]	In flux [$\times 10^{-5}$ Pa]	Deposition thickness of InN [nm]	Average height [nm]	Average diameter [nm]	Area density [cm^{-2}]	AFM image
1	490	5.0	2.1	7.49	50.8	2.4×10^{10}	Fig. 6(a)
2	480	7.0	5.8	9.86	36.9	5.0×10^{10}	Fig. 6(b)
3	470	7.0	5.8	3.77	27.3	2.2×10^{11}	Fig. 6(c) and (d)

section. The corresponding AFM images in Fig. 3(b) and (c) show the formation of dot structures whose density increased with increasing the InN deposition amount. Therefore, the formation of InN dots has been confirmed. Furthermore, these dots show a tendency to align along the $\langle 1\,1\,0 \rangle$ directions. This lateral ordering tendency can be observed from the early stage of the dot growth as shown in Fig. 3(b) and possibly originate from the step edges along the $\langle 1\,1\,0 \rangle$ direction which exist on the surface of c-GaN underlayers. Fig. 4 is a cross section profile of the surface at the dotted line indicated in Fig. 3(c), showing the good uniformity of the dot size and shape. Fig. 5(a) shows an AFM image of a sample grown with the relatively large InN deposition amount of 30 nm. Although some of dots start to coalesce and the size uniformity is degraded, dot structures covering the whole surface are still observed. Fig. 5(b) shows the XRD θ–2θ scan profile for this sample. The peaks observed at 35.8°, 39.8° and 42.9° correspond to c-InN (002), c-GaN (002) and MgO (0 0 2), respectively. The peak at 32.9° is from In (1 0 1) due to In metal droplets with diameters of 20–30 μm which precipitated on the surface during the growth or during the cooling process after the growth. Although In droplets were detected, no clear peak assigned to h-InN was found in the pattern. Therefore, it is confirmed that the InN dots take over the crystal structure of the GaN underlayer and have the cubic lattice structure.

3.2. *Control of dot size and density*

In order to control the dot size and density, we have investigated the effects of various growth conditions on the c-InN dot formation. Fig. 6 show AFM images ((a)–(c) 1 μm × 1 μm, (d) 300 nm × 300 nm, (d) is a magnified image of (c)) of c-InN dots which were grown under different growth conditions as summarized in Table 1.

The area densities of the obtained dots are also described in the table. Different growth conditions of substrate temperature, In flux and InN deposition amount resulted in a variety of different dot size and density. What to be noted here is that the tendency to align along the $\langle 1\,1\,0 \rangle$ directions is maintained under any growth condition. Generally, the increase of the substrate temperature and the decrease of the source flux lead

to the enhancement of the surface migration of growing species during MBE process. Thus, the migration length on the growing surface should be longer in the order of condition 1, condition 2 and condition 3. As can be seen in Fig. 6 and Table 1, the shorter migration length results in the smaller dot diameter and the higher dot density. These results mean that the formation of the c-InN dots is governed by a kinetic growth mechanism. Therefore, the density and the size of c-InN dots are well controlled by adjusting the growth conditions such as the growth temperature and the In flux, and a very high dot density of 2.2×10^{11} cm^{-2} has been successfully obtained at a growth temperature of 470 °C and In flux of 7.0×10^{-5} Pa.

4. Conclusion

We have successfully grown c-InN nano-scale dots on c-GaN underlayers. The samples were grown by RF-N_2 MBE on MgO substrates. Structural investigation by AFM, RHEED and XRD measurements indicated the formation of c-InN dots which showed a tendency to align along the $\langle 1\,1\,0 \rangle$ directions. The density and the size of dots were well controlled by varying the growth conditions such as the substrate temperature and the In flux and dots with a very high area density of 2.2×10^{11} cm^{-2} were successfully obtained at a growth temperature of 470 °C and an In flux of 7.0×10^{-5} Pa.

References

[1] B. Maleyre, O. Briot, S. Ruffenach, Journal of Crystal Growth 269 (2004) 15.
[2] E. Dimakis, A. Georgakilas, E. Iliopoulos, K. Tsagaraki, A. Delimitis, Ph. Komninou, H. Kirmse, W. Neumann, M. Androulidaki, N.T. Pelekanos, Physica Status Solidi C Current Topics in Solid State Physics 3 (2006) 3983.
[3] W. Ke, S. Lee, S. Chen, C. Kao, W. Houng, C. Wei, Y. Su, Journal of Alloys and Compounds 526 (2012) 119.
[4] S. Yoshida, Physica E: Low-dimensional Systems and Nanostructures 7 (2000) 907.
[5] T. Inoue, Y. Iwahashi, S. Oishi, M. Orihara, Y. Hijikata, H. Yaguchi, S. Yoshida, Physica Status Solidi C Current Topics in Solid State Physics 5 (2008) 1579.
[6] K. Nishida, Y. Kitamura, Y. Hijikata, H. Yaguchi, S. Yoshida, Physica Status Solidi B Basic Solid State Physics 241 (2004) 2839.
[7] H. Tsuchiya, K. Sunaba, S. Yonemura, T. Suemasu, F. Hasegawa, Japanese Journal of Applied Physics 36 (1997) L1.
[8] S. Sanorpim, E. Takuma, H. Ichinose, R. Katayama, K. Onabe, Physica Status Solidi B Basic Solid State Physics 244 (2007) 1769.
[9] T. Schupp, T. Meisch, B. Neuschl, M. Feneberg, K. Thonke, K. Lischka, D.J. As, Physica Status Solidi C Current Topics in Solid State Physics 8 (2011) 1495.
[10] S. Sanorpim, P. Jantawongrit, S. Kuntharin, C. Thanachayanont, T. Nakamura, R. Katayama, K. Onabe, Physica Status Solidi C Current Topics in Solid State Physics 6 (2009) S376.